

the National Science Foundation. P.F.B. is an Alfred P. Sloan Fellow and Camille and Henry Dreyfus Teacher-Scholar. We thank J. H. Black, W. F. Huebner, H. W. Kroto, A. L. Merts, R. E. Smalley, and H. A. Wootten for useful discussions. We also thank W. A. Lenz for assisting at the telescope. Part of this research was performed under the auspices of the U.S. Department of Energy. Acknowledgment

is made to the donors of the Petroleum Research Fund, administered by the American Chemical Society, for partial support of this work. Partial support also was provided by the Air Force Astronautics Laboratory grant F 04611-87-K-0020.

29 April 1988; accepted 27 July 1988

Solid-State Ice Volcanism on the Satellites of Uranus

DAVID G. JANKOWSKI AND STEVEN W. SQUYRES

Voyager images of the uranian satellites Ariel and Miranda show flow features with morphologies indicating that ice has been extruded to the satellites' surfaces in the solid state. These images provide the first observational evidence for solid-state ice volcanism in the solar system. Topographic profiles have been measured across a number of flow features on Ariel. With a simple model of extrusion, spreading, and cooling of a viscous flow, the initial viscosity of the flow material is found to have been no more than about 10^{16} poise, far lower than expected for H_2O ice at the ambient surface temperatures in the uranian system. Sharply reduced viscosities may have resulted from incorporation of ices like NH_3 or CH_4 in the uranian satellites.

ONE OF THE MOST INTERESTING results of the Voyager mission to Jupiter, Saturn, and Uranus has been the extent to which even small icy satellites of those planets have undergone geologic resurfacing (1-5). It generally has been uncertain, however, whether the resurfacing has taken place in the liquid or solid state. In the jovian system, buoyancy considerations seem to favor extrusion of warm, mobile ice rather than liquid water (6). However, no landforms clearly indicative of solid-state extrusion have been observed there. On the smaller saturnian satellites, mobility considerations favor extrusion of liquid (7), and the observed morphology is at least consistent with this interpretation. In the uranian system, there is morphologic evidence for extrusion in the solid state (5). In this report we consider this evidence, quantify the morphology of the flows, derive approximate viscosities at the time of extrusion, and consider the implications of these viscosities for the compositions and thermal histories of the uranian satellites.

The morphologic evidence for solid-state resurfacing on the uranian satellites is best developed on Ariel (Figs. 1 and 2). Much of the satellite's surface is transected by a pattern of linear graben-like canyons. On the floors of some of the grabens are deposits that have low crater densities compared to the rest of the satellite (8) and have topographic profiles that appear to be strikingly smooth and convex. They appear to steepen significantly at the margins, in what seem to

be flow fronts. Some flows contain medial grooves running parallel to the graben walls. The convex topography and the concentration of the deposits in grabens strongly suggest that these deposits are materials that were extruded to the surface in the solid state, probably in an extensional environment.

In some cases, the flows appear to have been confined by graben walls. In others, however, they clearly have not. Figure 1

shows an instance where the lateral extent of a flow within a canyon remains relatively constant along the canyon's length, whereas the width of the canyon changes from that of the flow to roughly three times it. Figure 2 shows an instance where a flow has spread out across a plains unit, partially burying an impact crater.

It is likely that the sources of most flows were linear fracture systems on the graben floors. This interpretation is supported by (i) the likelihood that extensional fractures associated with grabens would parallel the graben walls; and (ii) the apparent steep flow fronts and limited lateral extent of some flows, indicating that they spread a short distance laterally rather than flowing long distances parallel to the graben walls. In large terrestrial grabens, volcanism is commonly concentrated along vents near the graben axis (9-11); such may also be the case on Ariel. At least some of the medial grooves may be the juncture of two independent flows that have been extruded from parallel fractures on a graben floor, have spread laterally and met, but have not completely coalesced.

Evidence for solid-state resurfacing is also observed on Miranda (Fig. 3). Miranda's surface consists of two types of materials: an old, heavily cratered terrain and a younger terrain transected by a complex pattern of subparallel bands, scarps, and ridges. Areas of this younger terrain are known as "coronae." In some places where corona materials come into contact with the ancient heavily

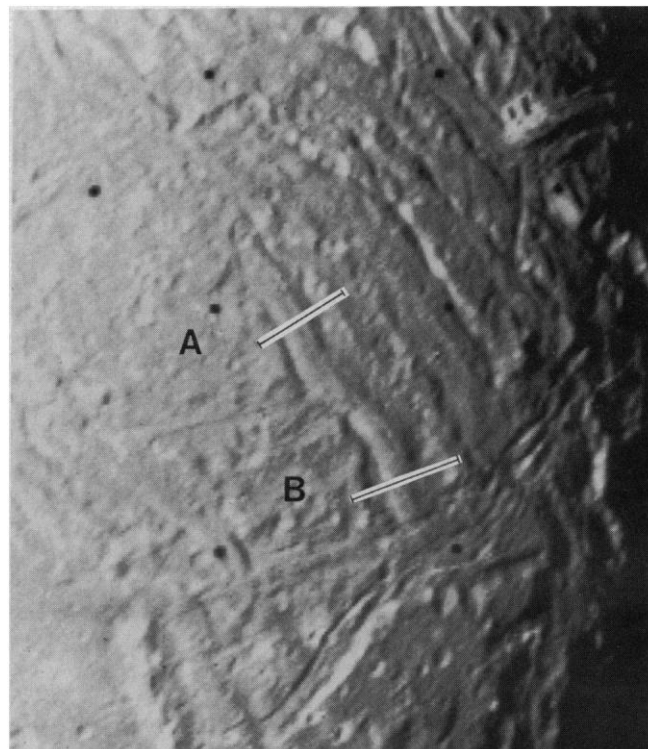


Fig. 1. Flow region near 30° south, 60° west. Photoclinometric scan lines are marked A and B.

cratered terrain, they exhibit distinct convex profiles like those at the margins of the flows on Ariel (12). As on Ariel, the most reasonable explanation of this morphology is that the convex profiles are flow fronts, and that the younger material was emplaced in the solid state.

Information about the rheologic properties of the flows may be inferred from the details of their topography. We have obtained topographic profiles across the flow

features using photogrammetry. Photogrammetry uses the photometric function of a surface and the known lighting geometry of an image to derive topographic slopes from surface brightness variations. It has been used successfully in a variety of planetary applications (13-16). To determine an accurate descriptive photometric function, a large number of intensity scans were taken along lines of constant photometric latitude in two Voyager 2 narrow angle-camera

clear-filter images of Ariel. The images used were the same ones used for the photogrammetry (FDS 26843.38 and 26845.33), with phase angles of 32° and 67°. The measured intensity scans were compared with the intensity variations predicted by two commonly used photometric functions, the Lommel-Seelinger and Minnaert functions. Calculating least-squares residuals, we found that the surface of Ariel in the region of the flows is fit best by the Minnaert function (intensity $I \propto \mu_0^k \mu^{k-1}$, where μ_0 is the cosine of the incidence angle and μ is the cosine of the emission angle) with a coefficient of $k = 0.85$.

Using the Minnaert function, we generated a number of photogrammetric profiles across flow features. Four are shown in Fig. 4. Linear resolutions along the profiles are in the range 1.0 to 1.5 km. Profile A shows topography across a flow that extends to the valley walls; profile B shows the same flow where the valley has widened. This flow feature is roughly 1.2 km in height and 20 km across, with a smooth, convex profile and a flat top. Profile C shows the topography across a flow on the floor of a wider valley. This flow is about 1 km in height and nearly 40 km across, and also has a smooth, convex topographic profile. Profile D shows the topography across a flow region containing a large medial groove. The entire flow region is about 50 km across and contains several rises ranging up to a height of about 0.8 km. Convex profiles are evident here as well. The morphology is consistent with the hypothesis that this medial groove results from partial flow coalescence.

An estimate of the viscosity of the extruded material can be determined from these topographic profiles with a simple analytical model. We consider the profile of a constant viscosity, incompressible, Newtonian fluid spreading on a flat surface under its own hydrostatic pressure (17). (A power-law rheology might be a more appropriate one to use under certain flow conditions, but a simple Newtonian model suffices to obtain an estimate of the mobility of the flows relative to their surroundings and to one another.) Since most of the flow features considered seem to originate from linear fluid flowing outward with Cartesian symmetry. Let $h(x,t)$ signify the height of the fluid at a distance x from the source at time t . Then the pressure in the fluid at a height z ($z \leq h$) is:

$$p = \rho g(h - z) \quad (1)$$

where ρ is the density of the fluid, g is the acceleration due to gravity for Ariel, and the pressure at the top of the fluid is taken to be zero. The equation of motion of the fluid

Fig. 2. Flow regions inside of Kewpie and Brownic chasmata. Photogrammetric scan lines are marked C and D. The arrow indicates a flow partially burying a crater.

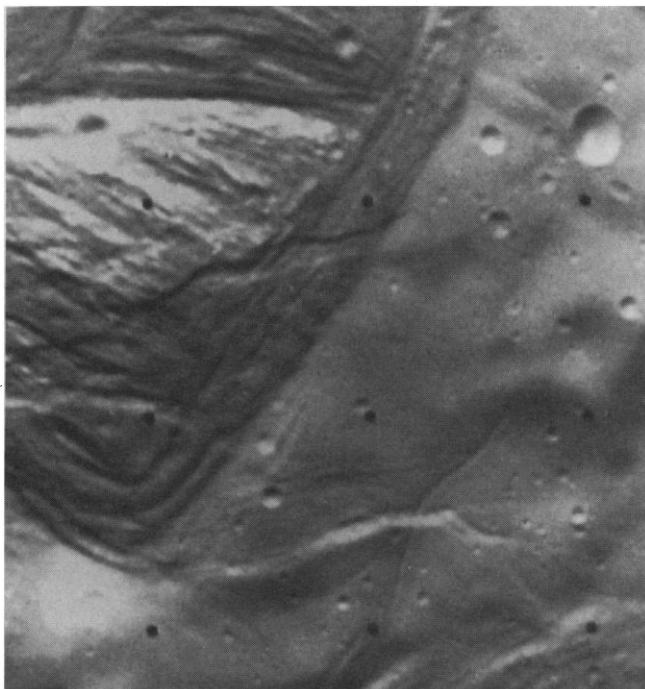
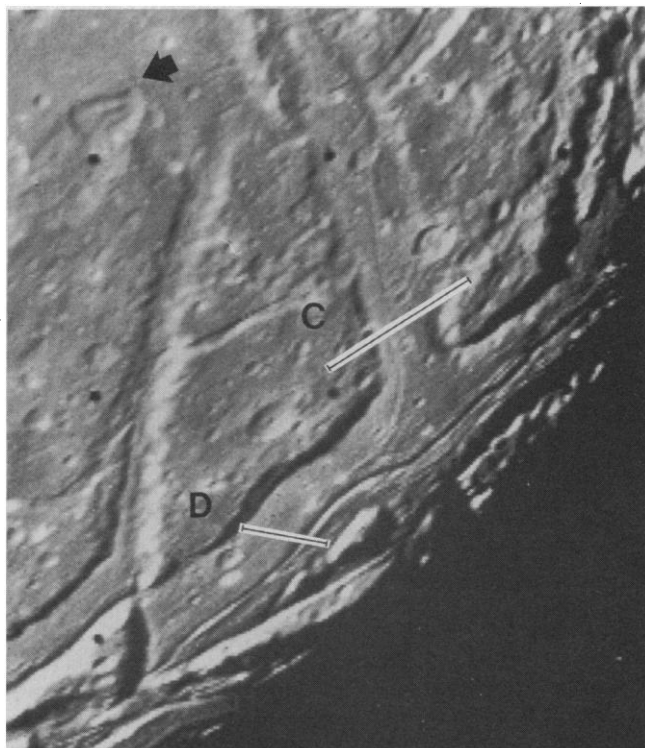


Fig. 3. Boundary between resurfaced terrain (upper left) and ancient cratered terrain on Miranda, showing the convex topographic front of the resurfaced terrain.

(neglecting viscous terms containing horizontal derivatives) is then given by:

$$\rho g \frac{\partial h}{\partial x} = \eta \frac{\partial^2 u}{\partial z^2} \quad (2)$$

where $u(x, z, t)$ is the horizontal velocity within the fluid and η is the fluid viscosity. Imposing no-slip conditions at the base of the fluid and zero stress at its top, the solution for the velocity is:

$$u(x, z, t) = -\frac{1}{2} \frac{\rho g}{\eta} \frac{\partial h}{\partial x} z(2h - z) \quad (3)$$

Another constraint upon u and h is imposed by fluid conservation through a vertical sheet (there are no sources or sinks of fluid except at $x = 0$):

$$\frac{\partial h}{\partial t} + \frac{\partial}{\partial x} \left[\int_0^h u(x, z, t) dz \right] = 0 \quad (4)$$

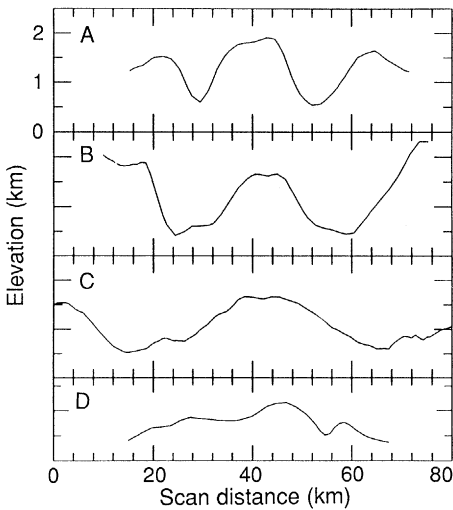


Fig. 4. Topographic profiles along the scan lines in Figs. 1 and 2. The vertical exaggeration is 10:1.

Combining Eqs. 3 and 4 gives the partial differential equation:

$$\frac{\partial h}{\partial t} - \frac{1}{3} \frac{\rho g}{\eta} \frac{\partial}{\partial x} \left(h^3 \frac{\partial h}{\partial x} \right) = 0 \quad (5)$$

We solve Eq. 5, using a similarity variable approach, for fluids with total volumes of the form:

$$V = St^\phi \quad (0 \leq \phi \leq 1) \quad (6)$$

where S is a constant. The case $\phi = 0$ corresponds to a constant volume fluid, whereas the case $\phi = 1$ corresponds to a flow with a constant source of fluid at $x = 0$. One boundary condition on Eq. 5 results from conservation of fluid at $x = 0$:

$$Q(t) = \int_0^h h(0, z, t) dz = -\frac{1}{3} \frac{\rho g}{\eta} h^3 \left(\frac{\partial h}{\partial x} \right)_{x=0}$$

where $Q(t)$ is the extrusion rate at time t . The other boundary condition results from conservation of fluid of the entire flow:

$$V(t) = \int_0^{x_0} h(x, t) dx \quad (8)$$

where $V(t)$ is the total volume of the flow at a time t , and x_0 is the location of the advancing fluid front.

To compare the calculated fluid profiles to the measured topographic profiles, we allow the fluid to spread for one cooling time, τ_c , defined as d^2/κ , where d is the present height of the flow and κ is the thermal diffusivity (taken to be that of H₂O ice). After one cooling time, we assume that the flow has cooled sufficiently that its viscosity has increased substantially and spreading has effectively stopped. The basis for this assumption

is the strong exponential dependence of ice viscosity on temperature (18). It should be noted that the spreading of a cooling flow may be controlled primarily by its colder, higher viscosity margins. Rapid cooling of the flow terminus might therefore halt motion before substantial cooling and stiffening of the interior. Our assumption therefore is conservative, since it places an upper limit on the viscosity of the extruded material.

Profiles were generated assuming a fluid extrusion rate that diminishes with time such that $\phi = 1/2$ in Eq. 6, with no extrusion after the flow stops at $t = \tau_c$. Model profiles were then compared with topographic data, leaving the flow volume and viscosity as free parameters. The best-fit profiles for five flows are shown in Fig. 5. Profiles 5D, top and bottom, correspond to regions of profile D on opposing sides of the medial groove. The model profiles fit well except at large slope angles where mass wasting processes may come into effect. The viscosity limits found, given in the figure, are all close to 10^{16} poises. Figure 5, profile A, also shows calculated profiles for viscosities one order of magnitude greater and less than the best-fit value, demonstrating that the flow viscosities are tightly constrained by fits to the topography.

The viscosities obtained are relatively insensitive to the functional form assumed for the extrusion rate. Taking two extremes of $\phi = 0$ (all of the fluid extruded instantaneously at the beginning of the flow) and $\phi = 1$ (a constant extrusion rate for the duration of the flow), we find viscosities that bracket those in Fig. 5 and differ by only about a factor of 2.

Ice viscosities in the range of 10^{16} poises are extraordinarily low by normal standards for the outer solar system and have important implications for the thermal history and composition of the uranian satellites. If the extruded material were taken to be pure H₂O ice with a Newtonian rheology, the viscosities found would indicate a temperature for the ice of about 240 K (18). This is about 170 K higher than equilibrium surface temperatures expected for these satellites. If the extrusions are indeed pure water ice, some mechanism must have heated the satellites' interiors a great deal at some time in the past. There are two serious problems with this hypothesis, however. First, it is not clear that adequate heat sources are available. Accretional heating for Ariel can produce subsurface temperatures as high as 215 K (19), but this heating is concentrated in a very brief period at the beginning of the satellite's history. Accretional heating for Miranda is substantially less. More recent tidal heating, although possible for Ariel

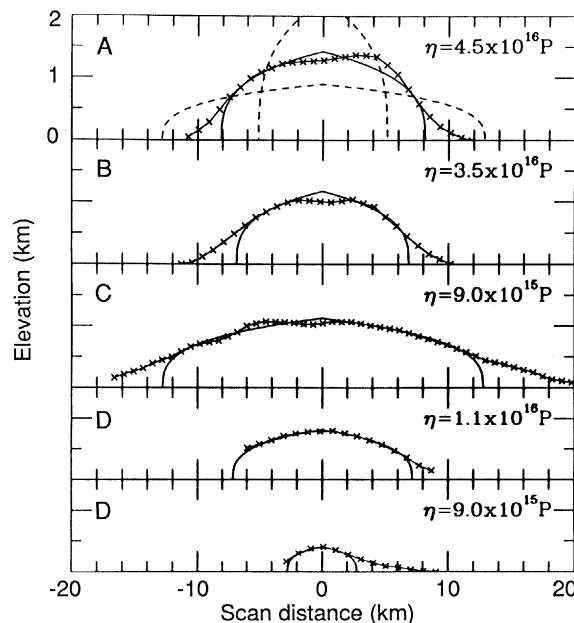


Fig. 5. Flow profiles from Fig. 4 (line with x's) and their best-fit model profiles (solid line). The vertical exaggeration is 5:1. The viscosity used to generate each model profile is shown. In profile A the dashed lines correspond to model profiles for viscosities one order of magnitude larger and smaller than the best-fit viscosity.

because of passage through a 5:3 resonance with Umbriel (20), is uncertain in both probability and magnitude. The same can be said for tidal heating of Miranda (21). A more serious problem is that it is difficult to imagine a global heating mechanism that could produce warming this great that would not lead to substantial viscous relaxation of nearby large impact craters and tectonic features that clearly predate the extrusion events (10-km craters would have viscously relaxed in ~100 years at such high temperatures). Instead, a low viscosity material appears to have been segregated somehow, and then mobilized by temperatures not warm enough to allow relaxation of surrounding terrain.

There are strong cosmochemical arguments that suggest that the uranian satellites may have formed under conditions that would have led to inclusion of volatiles such as CH₄, CO, or N₂ as clathrates, or NH₃ as one of the stoichiometric ammonia hydrates (22, 23). Even modest amounts of accretional heating could have created a subsurface zone in which partial melting produced CH₄, CO, or N₂ liquid, or a H₂O-NH₃ peritectic melt. These fluids, because of their mobility and contrast in density with the surrounding material, would tend to migrate, forming segregated pockets or magma bodies.

Stevenson and Lunine (24) have suggested that a small amount of CH₄, CO, or N₂ fluid could cause pressure solution creep of a fine-grained ice matrix, leading to viscosities as low as 10¹⁴ poise at uranian system temperatures. This mechanism is attractive, although it is untested and highly dependent upon grain sizes and grain boundary widths. Very recent experimental results indicate that the viscosity of H₂O-NH₃ ice can be substantially lower than that of pure H₂O ice at the same temperature (25). Peritectic-composition NH₃-H₂O solid consists of two stable phases, H₂O ice and ammonia dihydrate (NH₃·2H₂O). The low viscosity found experimentally for the mixture indicates a rheology dominated by a more mobile phase other than H₂O, probably dihydrate (though metastable monohydrate or glass might also be present). Even if segregated peritectic-composition pockets solidified after accretional heat was lost, then they might be remobilized in the solid state by a relatively mild tidal heating episode. Since complete differentiation of the uranian satellites is very unlikely, the material surrounding these pockets would be comparable in density to the bulk satellite value of about 1.6 g/cm³. Despite the fact that ammonia dihydrate is slightly more dense than pure water ice (26), the pockets would be buoyant relative to surrounding undifferentiated

material and would rise to the surface if sufficiently mobile. We note that further creep experiments on all of these exotic ices are sorely needed.

The solid-state resurfacing that has taken place on the uranian satellites is, to our knowledge, unique in the solar system. Highly localized ice flows with viscosities less than 10¹⁶ poise on satellites this cold appear to require the presence of some material that can substantially increase mobility. If this material is indeed some low-temperature condensate, then solid-state ice volcanism might also be found to be geologically important in the Neptune and Pluto systems.

REFERENCES

1. B. A. Smith *et al.*, *Science* **204**, 951 (1979).
2. ———, *ibid.* **206**, 927 (1979).
3. ———, *ibid.* **212**, 163 (1981).
4. ———, *ibid.* **215**, 504 (1982).
5. ———, *ibid.* **233**, 43 (1986).
6. R. L. Kirk and D. J. Stevenson, *Icarus* **69**, 91 (1987).
7. D. J. Stevenson, *Nature* **298**, 142 (1982).
8. J. B. Plescia, *ibid.* **327**, 201 (1987).
9. P. A. Mohr, *ibid.* **213**, 664 (1967).
10. B. C. King, in *African Magmatism and Tectonics*, T. N. Clifford and I. G. Gass, Eds. (Oliver and Boyd, Edinburgh, 1970), pp. 263–283.
11. B. H. Baker and L. A. J. Willimans, *Geol. Soc. Am. Spec. Paper* **136** (1972).
12. S. K. Croft, *Lunar Planet. Sci. Conf. (Abstr.)* **19**, 225 (1988).
13. R. L. Wildey, *Icarus* **25**, 613 (1975).
14. S. W. Squyres, *ibid.* **46**, 156 (1981).
15. P. A. Davis and L. A. Soderblom, *J. Geophys. Res.* **89**, 9449 (1984).
16. J. M. Moore, A. S. McEwen, E. F. Albin, R. Greeley, *Icarus* **67**, 181 (1986).
17. H. E. Huppert, J. B. Shepherd, H. Sigurdsson, R. S. J. Sparks, *Volcanol. Geothermal Res.* **14**, 199 (1982).
18. J. Weertman, in *Physics and Chemistry of Ice*, E. Whalley, S. J. Jones, L. W. Gold, Eds. (Royal Society of Canada, Ottawa, 1973), pp. 320–337.
19. S. W. Squyres, R. T. Reynolds, A. L. Summers, F. Shung, *J. Geophys. Res.* **93**, 8779 (1988).
20. W. C. Tittlemore and J. Wisdom, *Bull. Am. Astron. Soc.* **19**, 821 (1987).
21. S. F. Dermott, R. Malhotra, C. D. Murray, *ibid.*, p. 820.
22. J. S. Lewis, *Icarus* **15**, 175 (1971).
23. J. I. Lunine and D. J. Stevenson, *Astrophys. J. Suppl.* **58**, 493 (1985).
24. D. J. Stevenson and J. I. Lunine, *Nature* **323**, 46 (1986).
25. W. B. Durham, S. H. Kirby, L. A. Stern, *Lunar Planet. Sci. Conf.* **19**, 285 (1988).
26. S. K. Croft, J. I. Lunine, J. Kargel, *Icarus* **73**, 279 (1988).
27. We thank P. Thomas, W. R. Thompson, P. Helfenstein, and D. Turcotte for helpful discussions. This work was supported by the NASA Uranus Data Analysis Program.

21 March 1988; accepted 19 July 1988

Site-Specific Integration of H-ras in Transformed Rat Embryo Cells

W. GILLIES MCKENNA, KEN NAKAHARA, RUTH J. MUSCHEL

A karyotypic analysis was performed on seven independently derived clones of primary rat embryo cells transformed by the *ras* oncogene plus the cooperating oncogene *myc*. The transfected oncogenes were sometimes present in amplified copy number, with heterogeneity in the levels of amplification. Some chromosomal features, such as aberrantly banding regions and double-minute chromosomes, typical of cells carrying amplified genes, were also seen in three of the seven cell lines. Underlying this heterogeneity there was an unexpected finding. All seven lines showed a common integration site for *ras* on the q arm of rat chromosome 3 (3q12), though some lines also had other sites of integration. In four of the lines integration of *ras* was accompanied by deletion of the p arm of chromosome 3 or its possible translocation to chromosome 12.

ACTIVATION OF THE *ras* ONCOGENE has been implicated in a wide variety of human and animal malignancies (1). In NIH 3T3 cells the oncogene has been shown by calcium phosphate-DNA transfection to cause morphological transformation (2) and to induce the tumorigenic (3) and metastatic (4) phenotypes. Spandinos and Wilkie (5) have shown that it is possible to transform a variety of early passage cells with H-*ras* when the gene is linked to a strong enhancer. Similar results were reported for very early passage rat embryo

cells by Pozzatti *et al.* (6). The latter also showed that it was possible to obtain rare transformants with the *ras* gene alone (in co-transfection with a selectable marker, pRSVneo), if rat embryo fibroblasts were transfected when subconfluent. These rare

W. G. McKenna, Department of Radiation Oncology, University of Pennsylvania School of Medicine, Philadelphia, PA 19104.

K. Nakahara, NCI-Navy Medical Oncology Branch, Naval Hospital, Bethesda, MD 20895.

R. J. Muschel, Department of Pathology and Laboratory Medicine, University of Pennsylvania School of Medicine, Philadelphia, PA 19104.